

# G<sup>2</sup>VD Planner: Efficient Motion Planning With Grid-based Generalized Voronoi Diagrams

Jian Wen, Xuebo Zhang, *Senior Member, IEEE*, Qingchen Bi, Hui Liu, Jing Yuan, *Member, IEEE*,  
and Yongchun Fang, *Senior Member, IEEE*

**Abstract**—In this paper, an efficient motion planning approach with grid-based generalized Voronoi diagrams (G<sup>2</sup>VD) is newly proposed for mobile robots. Different from existing approaches, the novelty of this work is twofold: 1) a new state lattice-based path searching approach is proposed, in which the search space is reduced to a Voronoi corridor to further improve the search efficiency, along with a Voronoi potential field constructed to make the searched path keep a reasonable distance from obstacles to provide sufficient optimization margin for the subsequent path smoothing; 2) an efficient quadratic programming-based path smoothing approach is presented, wherein the clearance to obstacles is considered in the form of the penalty of the deviation from the safe reference path to improve the path clearance of hard-constrained path smoothing approaches. We validate the efficiency and smoothness of our approach in various challenging simulation scenarios and outdoor environments. It is shown that the computational efficiency is improved by 17.1% in the path searching stage, and path smoothing with the proposed approach is 25.3 times faster than an advanced sparse-banded structure-based path smoothing approach.

**Note to Practitioners**—This paper is motivated by the challenges of motion planning problems of mobile robots. An efficient motion planning approach called G<sup>2</sup>VD planner is proposed by combining path searching, path smoothing, and time-optimal velocity planning. Extensive simulation and experimental results show the effectiveness of the proposed motion planning approach. However, the prediction information of dynamic obstacles is not incorporated in the proposed motion planner, thus the motion planner may be a bit sluggish in response to dynamic obstacles. In future research, we will concentrate on extending the proposed motion planning approach with the theory of partially observable Markov decision process (POMDP) to deal with the uncertainty of dynamic obstacles.

**Index Terms**—Autonomous navigation, mobile robots, motion planning, path planning, path optimization

## I. INTRODUCTION

MOBILE robots have been widely applied in various fields including but not limited to intelligent inspection, logistics, and search-and-rescue applications. Motion planning is one of the key technologies for mobile robots to achieve full autonomy in these scenarios and plays an essential role in generating safe, smooth, and efficient motions [1]–[3].

This work is supported in part by National Key Research and Development Project under Grant 2018YFB1307503, in part by Tianjin Science Fund for Distinguished Young Scholars under Grant 19JCJC62100, and in part by the Fundamental Research Funds for the Central Universities. (*Corresponding author: Xuebo Zhang.*)

The authors are with the Institute of Robotics and Automatic Information System, College of Artificial Intelligence, Nankai University, Tianjin 300350, China, and also with the Tianjin Key Laboratory of Intelligent Robotics, Nankai University, Tianjin 300350, China (e-mail: zhangxuebo@nankai.edu.cn; wenjian@mail.nankai.edu.cn).

Although plenty of works on motion planning of mobile robots have been put forward, it is still challenging to design a motion planning approach that can ensure both efficiency, safety, and smoothness in complex environments [4]–[7].

### A. Path Searching

Many path searching approaches have been proposed in terms of different theories [8], which can be classified into three categories. The sampling-based planning algorithms such as the famous probabilistic roadmap (PRM) [9] and rapidly-exploring random trees (RRTs) [10] have gained popularity for the capability of efficient searching in the configuration space (C-space). However, they are limited by completeness and optimality, and even some excellent variants such as RRT\* [11] can only guarantee asymptotic optimality. The classical artificial potential field (APF) algorithm [12] finds a feasible path by following the steepest descent of a potential field. However, the APF often suffers from the local minimum problem. In this paper, we focus on grid-based planning algorithms. Grid-based planning overlays a hyper-grid on the C-space and assumes each configuration is identified with the grid-cell center. Then, search algorithms are used to find a path from the start to the goal. Grid-based planning can always find a resolution-optimal path if it exists in the discrete search space, namely, completeness and optimality in the sense of resolution are guaranteed. However, these approaches depend on space discretization and do not perform fast as the environment dimension increases.

### B. Path Smoothing

The path obtained by path searching approaches usually fails to meet the smoothness requirement for robot navigation and needs further smoothing [13]. Two types of path smoothing approaches are investigated in this paper, namely, soft-constrained approaches and hard-constrained approaches.

1) *Soft-constrained Approaches*: These approaches formulate path smoothing as a non-linear unconstrained optimization problem, wherein the constraints are considered in the optimization objective in the form of penalty cost terms [14]–[16]. Generally, the smoothness of the path and the clearance to obstacles are both taken into account. Then, gradient-based optimization algorithms are employed to solve the problem. Soft-constrained approaches utilize gradient information to push the path far from obstacles and can obtain a smooth path with a reasonable distance from obstacles. However, it is difficult for these approaches to guarantee the optimized path

strictly satisfies the constraints. In addition, the optimization objective of soft-constrained approaches contains convex and non-convex terms, making these approaches suffer from local optima and time-consuming issues [17].

2) *Hard-constrained Approaches*: These approaches formulate path smoothing as a non-linear constrained optimization problem and can obtain a path that theoretically satisfies the constraints [18], [19]. The optimization objective usually considers the smoothness or the length of the path and thus is convex. This convexity allows the problem to be solved efficiently [20], [21]. However, hard-constrained approaches treat all free space equally, namely, distance from feasible paths to obstacles is ignored. As a result, the optimized path is often close to the obstacle and has poor safety.

### C. Contributions

Motivated by the aforementioned limitations of existing works, an efficient motion planning approach called G<sup>2</sup>VD planner is newly proposed. Specifically, a grid-based generalized Voronoi diagram (G<sup>2</sup>VD) is utilized to aid path searching and path smoothing to achieve better performance in terms of computational and motion efficiency, safety, smoothness, etc.

1) *Path Searching*: Given the start and the goal, we first employ the A\* search to find the shortest grid path in a grid-based GVD. This shortest Voronoi path contains the topological information of the search direction and provides rough guidance for the subsequent fine search. Along the Voronoi grid path, a region called *Voronoi corridor* is proposed and constructed by adding a bounding box to each path pixel. Furthermore, the cost function of path searching is redesigned based on a potential called *Voronoi field* to make the searched path keep a reasonable distance from obstacles. Finally, the A\* search combined with motion primitives is utilized to finely search a kinematically feasible path within the Voronoi corridor. Different from the original state lattice-based path planner [22] that takes the whole grid map as the search space, the proposed approach reduces the search space to the Voronoi corridor, thus considerable time is saved for path searching. In addition, the certain clearance to obstacles provides sufficient optimization margin for further path smoothing.

2) *Path Smoothing*: Taking the path searched above as the reference path, an efficient quadratic programming (QP)-based path smoothing approach is proposed, wherein the smoothness of the path and the deviation from the reference path are both considered in the optimization objective. Our goal is to obtain a smooth path while minimizing the deviation between the optimized path and the reference path. Because the reference path searched above has a certain distance to obstacles, the clearance to obstacles is implicitly considered in the proposed approach, and the path clearance issue of such a hard-constrained approach is addressed. This is also the second reason why we introduce the Voronoi field and redesign the cost function of path searching to improve the path clearance of the searched path, in addition to providing wider optimization margin for path smoothing.

To summarize, the main contributions of this work are as follows:

- 1) A new state lattice-based path searching approach is proposed, in which a novel Voronoi corridor is introduced to reduce the search space to significantly improve the search efficiency, along with a Voronoi potential constructed to make the searched path keep a reasonable distance from obstacles to provide sufficient optimization margin for further path smoothing.
- 2) A new QP-based path smoothing approach is presented to efficiently smooth the searched path, wherein the clearance to obstacles is considered in the form of the penalty of the deviation from the safe reference path to address the path clearance issue of existing hard-constrained path smoothing approaches.
- 3) Autonomous navigation is realized in outdoor environments. Extensive simulation and experimental evaluations are presented to validate the effectiveness of the proposed approach.

The rest of this paper is organized as follows. We first review the related work in Section II. The proposed G<sup>2</sup>VD planner is detailed in Section III. Section IV provides some implementation details. The results of simulations and experiments are presented in Sections V and VI, respectively. Finally, this paper is concluded in Section VII.

## II. RELATED WORK

Grid-based planning obtains the resolution-optimal path by discretizing the C-space first and then using graph search algorithms to find the path. However, original grid-based planning approaches only visit the centers of grid cells and produce piecewise-linear paths that do not generally satisfy the kinodynamic constraints of the robot. To address this problem, Pivtoraiko *et al.* [23] propose the state lattice approach for graph construction. In particular, the connectivity between two nodes in the graph is built from a pre-designed motion primitive that fulfills the kinodynamic constraints of the robot. Based on the work [23], Likhachev *et al.* present a state lattice-based path planner by combining AD\* search with motion primitives [22], which has been successfully applied in the DARPA Urban Challenge [24]. In this paper, a new state lattice-based path planner is proposed, wherein the search space is reduced to a Voronoi corridor derived based on a generalized Voronoi diagram (GVD) to further improve the search efficiency.

The use of GVDs has long been proposed in the context of robot motion planning. In [25], Choset and Burdick use the GVD to derive skeletons of the free space and then search on the graph. However, the shortest Voronoi path may be far from the actual optimal path. In [26], Ziegler *et al.* utilize the GVD to inform the A\* search by constructing a heuristic where the cost of a search state is the sum of the straight-line path to the nearest Voronoi edge and the shortest path along the GVD edges. However, the resulting heuristic cannot be guaranteed to be admissible since the cost of the shortest Voronoi path may be greater than that of the actual shortest path. In [27], Dolgov *et al.* design a potential field based on the GVD for path smoothing. This potential allows precise navigation in narrow passages while also effectively pushing

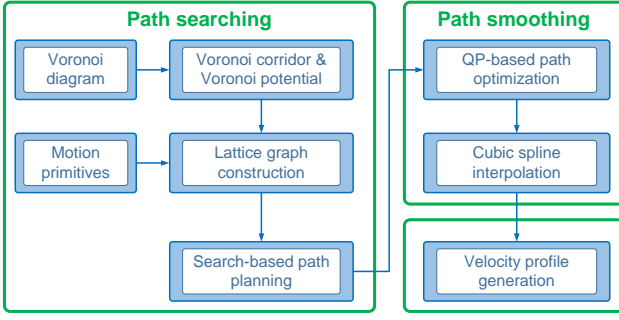


Fig. 1. Flow chart of the proposed three-layer motion planning framework.

the robot away from obstacles in wider areas. Inspired by the Voronoi field, we redesign the cost function of the state lattice-based path planner to obtain a path with a reasonable distance from obstacles.

The path obtained by path searching approaches usually needs further smoothing. In [27], Dolgov *et al.* present a conjugate gradient (CG)-based path smoothing approach to smooth the path generated by the hybrid A\* algorithm. In [28], Wen *et al.* propose a gradient-based local path smoothing approach for mobile robots, wherein the sparse-banded system structure of the underlying optimization problem is fully exploited to efficiently solve the problem. The above soft-constrained approaches utilize gradient information to push the path far from obstacles and can obtain a path with better safety. However, it is difficult for these approaches to guarantee the optimized path strictly satisfies the constraints. Recently, Zhou *et al.* propose a dual-loop iterative anchoring path smoothing (DL-IAPS) approach for autonomous driving [29], in which the nonlinear curvature constraint is linearized and sequential convex programming (SCP) is used to efficiently solve the path optimization problem. Such a hard-constrained approach can theoretically guarantee that the obtained path strictly satisfies the constraints. However, distance from feasible paths to obstacles is ignored, which often results in the optimized path being close to obstacles and poor safety. In this paper, a new QP-based path smoothing approach is proposed, in which the clearance to obstacles is implicitly considered in the form of the penalty of the deviation from the safe reference path to improve the path clearance of hard-constrained approaches.

### III. G<sup>2</sup>VD PLANNER

In this paper, a three-layer motion planning framework called G<sup>2</sup>VD planner is carefully designed, which consists of path searching, path smoothing, and velocity planning, as shown in Fig. 1. The path searching module is utilized to provide a safe reference path for the robot, and the path smoothing module combined with our previously proposed time-optimal velocity planning [30] is employed to generate safe, smooth, and efficient motion commands. In this section, we will detail the newly proposed path searching and path smoothing modules.

#### A. Grid-based Generalized Voronoi Diagrams

The GVD is defined as the set of points in the free space to which the two nearest obstacles have the same distance

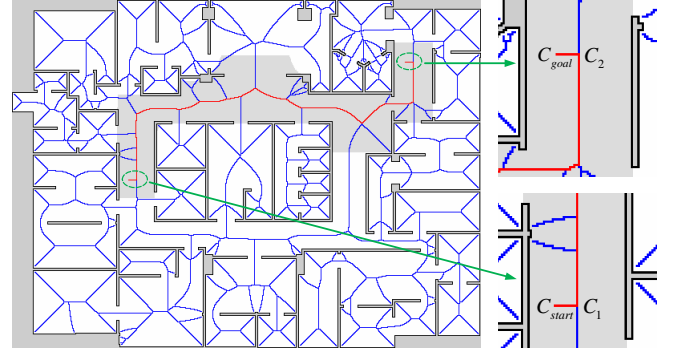


Fig. 2. Grid-based GVD of an office-like environment. The GVD edge pixels are colored in blue and red, and the searched shortest Voronoi path is colored in red. The gray region surrounding the Voronoi path denotes the Voronoi corridor.

[25]. In this paper, an efficient, incrementally updatable GVD construction algorithm presented in [31] is utilized to convert the occupancy grid map to a GVD in discrete form. This algorithm [31] employs a wavefront algorithm to perform distance transforms. Therefore, every cell in the grid-based GVD stores not only the state of whether it belongs to the GVD but also the minimum Euclidean distance to the nearest obstacle cell. Fig. 2 illustrates the grid-based GVD of an office-like environment, in which the GVD edge pixels are colored in blue and red.

#### B. Voronoi Corridor

After obtaining the grid-based GVD, breadth-first search is employed to find the cells  $C_1$  and  $C_2$  nearest to the start cell  $C_{start}$  and the goal cell  $C_{goal}$  on the GVD, respectively. And the shortest grid paths  $L_1$  from  $C_{start}$  to  $C_1$  and  $L_2$  from  $C_2$  to  $C_{goal}$  are also computed in this process. Then, the A\* search is utilized to search the shortest grid path  $L_3$  from  $C_1$  to  $C_2$  along the GVD edge pixels, in which collision detection is carried out based on the circumscribed radius of the robot. In particular, the cells whose distance to the nearest obstacle is less than the circumscribed radius of the robot are considered invalid and eliminated. Therefore, the final searched 2-D grid path consisting of valid cells is guaranteed to be collision-free. As shown by the red path in Fig. 2, the final shortest Voronoi path from  $C_{start}$  to  $C_{goal}$  is composed of  $L_1$ ,  $L_3$ , and  $L_2$ .

Based on the shortest Voronoi grid path searched above, a region called Voronoi corridor is constructed as follows. For every cell  $C_k$  in the shortest Voronoi grid path, the minimum distance to the nearest obstacle cell  $d_k$  is retrieved from the grid-based GVD. Then, a square bounding box with a side length of  $2d_k$  is centered on  $C_k$ . The obstacle-free cells covered by all bounding boxes make up the Voronoi corridor, as illustrated by the gray region in Fig. 2.

#### C. Path Searching

The shortest Voronoi path is far from the actual optimal path, and its piecewise-linear form also does not satisfy the kinodynamic constraints of the robot. To address these issues, a new state lattice-based path planner is proposed to perform fine path searching within the Voronoi corridor.

A typical state lattice-based path planner consists of two parts, namely, graph construction and graph search [22]. As for graph construction, the 3-D search space  $(x, y, \theta)$  is discretized first, where  $(x, y)$  denotes the position of the robot in the world and  $\theta$  represents the heading of the robot. In particular, the orientation space is discretized into 16 angles. Furthermore, the connectivity between two states in the graph is built from motion primitives which fulfill the kinematic constraints of the robot. In this work, a quintic Bézier curve-based path generation approach described in [30] is employed to generate motion primitives from each discretized angle offline. A motion primitive  $\gamma(s_1, s_n)$  consists of a sequence of internal robot poses  $\{s_1, s_2, \dots, s_n\}$ ,  $s_i = (x_i, y_i, \theta_i)$ ,  $1 \leq i \leq n$  when moving from state  $s_1$  to state  $s_n$ , where  $n$  is the number of poses contained in the motion primitive. As for graph search, the standard A\* search is employed, where the 2-D heuristic  $h_{2D}$  proposed in [22] is utilized to guide the A\* search away from those areas with dead-ends.  $h_{2D}$  is constructed by computing the costs of shortest 2-D grid paths from the goal cell to other cells in the search space through dynamic programming. In addition, since the motion primitives from each discretized angle are designed offline in advance, the covered cells of each motion primitive considering the robot footprint can be also computed and recorded as a lookup table in advance at the origin  $(0, 0)$ . During every A\* expansion, the covered cells of the selected motion primitive are retrieved in the lookup table and translated according to the robot position. As long as one of the covered cells is occupied by obstacles, the corresponding motion primitive is considered invalid and eliminated in this expansion. Therefore, the final searched path consisting of valid motion primitives is guaranteed to be collision-free.

Different from the original state lattice-based path planner [22] that takes the whole grid map as the search space, we reduce the search space to the Voronoi corridor to further improve the search efficiency. In addition, every time the grid map is updated,  $h_{2D}$  needs recalculation before performing path searching. Since the search space of the newly proposed state lattice-based path planner is reduced to the Voronoi corridor, dynamic programming is accordingly limited to only compute the costs of shortest paths from the goal cell to those cells that are within the Voronoi corridor. Therefore, considerable time is also saved for the recalculation of  $h_{2D}$ .

Although the path searched above is optimal in the search space, it may be very close to obstacles since only the path length is considered in the cost function. The ideal path is to keep a reasonable distance from obstacles to provide sufficient optimization margin for subsequent path smoothing. To this end, inspired by the Voronoi field presented in [27], we design the following potential function

$$\rho_V(x, y) = \begin{cases} \frac{d_V(x, y)}{d_O(x, y) + d_V(x, y)} \frac{(d_O - d_O^{\min})^2}{(d_O^{\min})^2} & d_O \leq d_O^{\min} \\ 0 & d_O > d_O^{\min} \end{cases}, \quad (1)$$

where  $d_V(x, y)$  and  $d_O(x, y)$  denote the distances from the given path vertex  $(x, y)$  to the nearest Voronoi edge and the

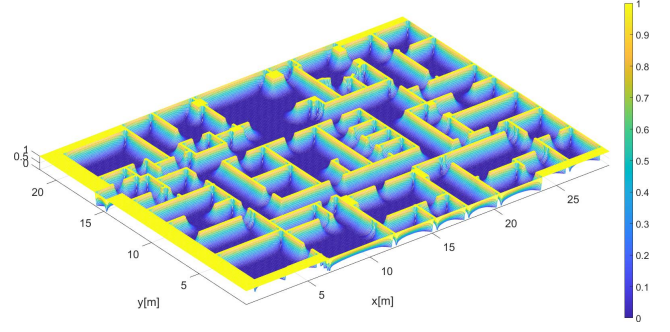


Fig. 3. Illustration of the Voronoi field of the office-like environment shown in Fig. 2. The light yellow regions are obstacle areas.

nearest obstacle, respectively.  $d_O^{\min}$  is a threshold specifying the minimum safety distance to obstacles. An example of the Voronoi field is shown in Fig. 3.

According to [27], this potential function has the following properties:

- i)  $\rho_V(x, y) \in [0, 1]$  and is continuous on  $(x, y)$  since we cannot simultaneously have  $d_V = 0$  and  $d_O = 0$ ;
- ii)  $\rho_V(x, y)$  reaches its maximum only when  $(x, y)$  is within obstacle areas;
- iii)  $\rho_V(x, y)$  reaches its minimum only when  $(x, y)$  is on the edges of the GVD or the distance from  $(x, y)$  to the nearest obstacle is greater than  $d_O^{\min}$ .

It is noteworthy that the potential cost is set to zero when the distance to the nearest obstacle is greater than the safety threshold ( $d_O > d_O^{\min}$ ). The reason for this design is as follows. Our goal is to make the searched path close to Voronoi edges through the Voronoi field so that the obtained path can keep an appropriate distance from obstacles and provide sufficient optimization margin for subsequent path smoothing. However, if the environment is wider and the Voronoi edge is far from the obstacles on both sides, which may make the searched path far away from the optimal path. Therefore, we set a safety distance threshold  $d_O^{\min}$  and regard the area where the distance to the nearest obstacle exceeds  $d_O^{\min}$  as a safe region. In this way, the searched path can keep a certain distance from obstacles and will not be far away from the optimal path through the Voronoi field.

Based on the above Voronoi field, the cost of motion primitives is defined as follows. For the sake of computational efficiency, we broadly follow the work [27] and temporarily assume that the robot travels at constant linear and angular velocities. If a motion primitive  $\gamma(s_1, s_n)$  collides with obstacles, the cost  $g(\gamma(s_1, s_n))$  is set to infinity. Otherwise, the cost of this motion primitive is defined as

$$g(\gamma(s_1, s_n)) = t(s_1, s_n) \cdot \left( \max_{(x, y) \in \mathcal{Q}} \rho_V(x, y) + 1 \right), \quad (2)$$

where  $t(s_1, s_n)$  is the minimum travel time spent on  $\gamma(s_1, s_n)$  assuming uniform motion under the constraints of the maximum linear velocity  $v_{\max}$  and the maximum angular velocity  $\omega_{\max}$

$$t(s_1, s_n) = \max \left\{ \frac{\sum_{i=1}^{n-1} \|s_{i+1} - s_i\|}{v_{\max}}, \frac{|\theta_n - \theta_1|}{\omega_{\max}} \right\}. \quad (3)$$

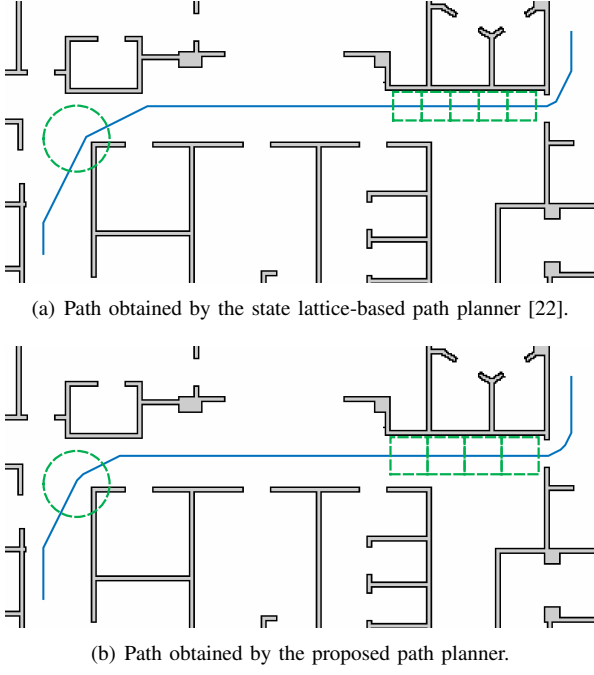


Fig. 4. Illustration of path searching results.

$\mathcal{Q}$  is the set of 2-D cells covered by the robot when moving from state  $s_1$  to state  $s_n$ . Intuitively, the Voronoi field penalizes slightly more those actions for which the robot traverses high potential cost areas (e.g., obstacles) and makes the searched path as close as possible to the Voronoi edges or keep a certain distance from obstacles. In addition, the 2-D heuristic  $h_{2D}$  is also multiplied by the potential costs to be consistent with the cost definition of motion primitives.

*Remark:* In general, the path length is considered in the cost function of path planning approaches. However, the action of rotation in place is contained in the designed motion primitives in this work since our platform is a differential-drive mobile robot. And the cost of this action will be 0 if the cost function of the motion primitive is defined as the path length. Therefore, the travel time spent on the motion primitive is considered in the cost function instead of the path length in this work.

It should be noted that the Voronoi potential field in [27] is used for path smoothing and the region of interest is the whole map. While the search space of the newly proposed state lattice-based path planner is reduced to the Voronoi corridor, and we only need to compute the Voronoi potential costs within the Voronoi corridor. In particular, an efficient distance transform algorithm presented in [32] is employed to compute the Euclidean distance to the nearest Voronoi edge for those cells within the Voronoi corridor. Figs. 4(a) and 4(b) illustrate the paths searched by the original state lattice-based path planner [22] and the newly proposed path planner, respectively. Compared with the original state lattice-based path planner, the path obtained by the proposed path planner has a certain distance from obstacles and can provide wider optimization margin (green bounding boxes) for further path smoothing, which will be detailed in Section III-D.

*Remark:* The final path is found within the Voronoi corridor,

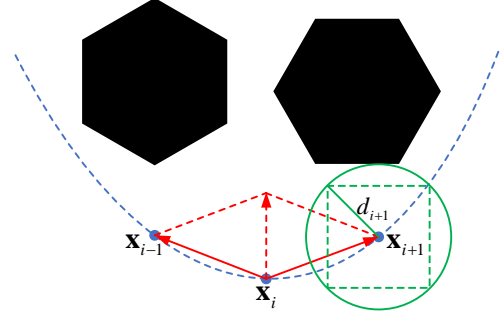


Fig. 5. Illustration of path smoothing formulation.  $\mathbf{x}_{i-1}$ ,  $\mathbf{x}_i$ , and  $\mathbf{x}_{i+1}$  denote three successive path vertices.  $d_{i+1}$  is the distance from  $\mathbf{x}_{i+1}$  to the nearest obstacle. The black blocks represent obstacles.

namely, the final solution is searched in a subset of the complete solution set to achieve high computational efficiency performance. The Voronoi corridor is generated based on the shortest Voronoi path searched in the grid-based GVD and usually contains the optimal solution in the complete solution set. However, when there is a significantly large difference in the dimension of the environment, it is possible that the optimal solution is contained in a sub-optimal Voronoi corridor derived based on a sub-optimal Voronoi path. Therefore, we cannot theoretically guarantee the optimality of the proposed approach. However, the practical performance is satisfactory, which is demonstrated through extensive simulation and experimental tests in Sections V and VI.

#### D. Path Smoothing

The path obtained by the state lattice-based path planner is kinematically feasible, but it is still piecewise-linear and not suitable for velocity planning. Therefore, an efficient QP-based path smoothing approach combined with cubic spline interpolation is employed to further smooth the path.

The input of path smoothing is several reference path vertices obtained by sampling in the path generated by the state lattice-based path planner with a fixed interval. In consideration of the smoothness of the path and the deviation from the reference path, a convex QP-based path smoothing formulation is defined as

$$\min_{\mathbf{x}} \omega_s \sum_{i=2}^{n-1} \|\mathbf{x}_{i+1} - 2\mathbf{x}_i + \mathbf{x}_{i-1}\|^2 + \omega_r \sum_{i=1}^n \|\mathbf{x}_i - \mathbf{x}_{i_{ref}}\|^2, \quad (4)$$

subject to

$$\mathbf{x}_1 = \mathbf{x}_{1_{ref}} \text{ and } \mathbf{x}_n = \mathbf{x}_{n_{ref}}, \quad (5a)$$

$$\mathbf{x}_i \in \mathcal{B}_i, \text{ for } i = 2, \dots, n-1, \quad (5b)$$

where  $\mathbf{x} = [\mathbf{x}_1^T \mathbf{x}_2^T \dots \mathbf{x}_n^T]^T$  is a  $2n$ -dimensional parameter vector, and  $\mathbf{x}_i = (x_i, y_i)^T$ ,  $1 \leq i \leq n$  denotes the world coordinates of a path vertex.  $\mathbf{x}_{i_{ref}} = (x_{i_{ref}}, y_{i_{ref}})^T$ ,  $1 \leq i \leq n$  is the corresponding reference path vertex of  $\mathbf{x}_i$ , and  $\omega_s$  and  $\omega_r$  are the weights of cost terms.  $\mathcal{B}_i$  is a state bubble constraining the feasible region of the path vertex  $\mathbf{x}_i$ . In this work,  $\mathcal{B}_i$  is approximated as an inscribed square of a circle centered on  $\mathbf{x}_{i_{ref}}$ , where the radius of the circle is equal to the distance



$d_i$  from  $\mathbf{x}_{i_{ref}}$  to the nearest obstacle minus the circumscribed radius  $r_c$  of the robot, as shown in Fig. 5. Therefore,  $\mathbf{x}_i \in \mathcal{B}_i$  in Eq. (5b) is approximated as

$$x_{i_{ref}} - b_i \leq x_i \leq x_{i_{ref}} + b_i, \quad (6a)$$

$$y_{i_{ref}} - b_i \leq y_i \leq y_{i_{ref}} + b_i, \quad (6b)$$

where the optimization margin  $b_i$  is defined as

$$b_i = \begin{cases} \frac{\sqrt{2}}{2}d_i - r_c & \frac{\sqrt{2}}{2}d_i > r_c \\ 0 & \frac{\sqrt{2}}{2}d_i \leq r_c. \end{cases} \quad (7)$$

Based on the constraints in Eqs. (6) and (7), the distance between every optimized path vertex and the corresponding nearest obstacle is greater than the circumscribed radius of the robot, thus the final smoothed path is guaranteed to be collision-free. According to Eq. (7), a path vertex  $\mathbf{x}_i$  will be fixed during the optimization process if the corresponding reference path vertex  $\mathbf{x}_{i_{ref}}$  is close to the obstacle ( $\frac{\sqrt{2}}{2}d_i \leq r_c$ ). Intuitively, a reference path with a certain distance from obstacles can provide sufficient optimization margin for path smoothing. This is one of the main reasons why we introduce the Voronoi field and redesign the cost function of path searching to make the searched path keep a reasonable distance from obstacles in Section III-C.

The first term in Eq. (4) is a measure of the path smoothness. The cost function  $\mathbf{x}_{i+1} - 2\mathbf{x}_i + \mathbf{x}_{i-1}$  can be rewritten as  $(\mathbf{x}_{i+1} - \mathbf{x}_i) + (\mathbf{x}_{i-1} - \mathbf{x}_i)$ . As shown in Fig. 5, from a physical point of view, this cost term treats the path as a series spring system, where  $\mathbf{x}_{i+1} - \mathbf{x}_i$  and  $\mathbf{x}_{i-1} - \mathbf{x}_i$  are the forces on the two springs connecting the vertices  $\mathbf{x}_{i+1}$ ,  $\mathbf{x}_i$  and  $\mathbf{x}_{i-1}$ , respectively. If the forces  $\mathbf{x}_{i+1} - \mathbf{x}_i$  and  $\mathbf{x}_{i-1} - \mathbf{x}_i$  are equal in size and opposite in direction, the resultant force  $(\mathbf{x}_{i+1} - \mathbf{x}_i) + (\mathbf{x}_{i-1} - \mathbf{x}_i)$  is a zero vector and the norm is minimum. If all the resultant forces are zero vectors, all the vertices would uniformly distribute in a straight line, and the path is ideally smooth.

The second term in Eq. (4) is used to penalize the deviation from the original safe reference path. As mentioned before, the hard-constrained formulation does not explicitly consider the path clearance, namely, distance from feasible paths to obstacles is ignored. As a result, the optimized path may be close to obstacles. To address this issue, the penalty of the deviation from the original reference path is introduced in the optimization objective. Our goal is to obtain a smooth path while minimizing the deviation between the optimized path and the reference path. Because the reference path searched by the proposed state lattice-based path planner has certain clearance to obstacles, the safety of the path is implicitly considered in the optimization formulation, and the final optimized path will not be close to obstacles. This is also the second reason why we introduce the Voronoi field and redesign the cost function of path searching to improve the path clearance of the searched path, in addition to providing wider optimization margin for path smoothing.

### E. Velocity Profile Generation

After path optimization, a path that is much smoother than the original reference path is obtained. However, the number of the path vertices is the same as that of the input reference path and the optimized path is still piecewise-linear. Therefore, we further smooth the path via cubic spline interpolation to obtain a continuous curve. Finally, a numerical integration (NI)-based time-optimal velocity planning algorithm presented in [30] is employed to generate a feasible linear velocity profile along the smoothed local path. The NI-based algorithm can acquire a provably time-optimal trajectory with low computational complexity [33]–[35]. Readers can refer to [30] for more details about the proofs of feasibility, completeness, and time-optimality of this algorithm.

## IV. IMPLEMENTATION DETAILS

### A. Setup

G<sup>2</sup>VD planner is implemented in C/C++. The convex QP problem described in Section III-D is solved by an alternating direction method of multipliers (ADMM)-based QP solver, OSQP [36]. The reference path vertices of path smoothing are obtained by sampling in the path generated by the state lattice-based path planner with an interval of 0.1 m. Densely sampling vertices along the path will introduce more optimization variables and increase the computational burden. In this work, the sampling interval is set according to the resolution of the underlying grid-based generalized Voronoi diagram and the dimension of the robot. The weights  $\omega_s$  and  $\omega_r$  are empirically set to 10 and 1, respectively. In the future, we plan to use machine learning techniques to tune these weights adaptively.

### B. Metrics

The proposed Voronoi corridor is integrated into the original state lattice-based path planner (A\* + motion primitives) [22] to derive a new state lattice-based path planner (A\* + motion primitives + Voronoi corridor). And the new path planner is compared with the original state lattice-based path planner to validate the effectiveness of the Voronoi corridor. The performance of path searching approaches is evaluated in terms of *computational efficiency* and *memory consumption*. In particular, the number of expanded states and the planning time are used to evaluate the computational efficiency, and the graph size, i.e., the number of created nodes in the search graph, is used to evaluate the memory consumption.

*Remark:* The runtime of the proposed path searching approach includes three parts: searching the shortest Voronoi grid path, constructing the Voronoi corridor, and searching the kinematically feasible path within the Voronoi corridor. In this work, the incrementally updatable GVD construction algorithm [31] is integrated into the mapper module. Therefore, the time used to construct the grid-based GVD is not included in the runtime of the proposed path searching approach.

To validate the effectiveness of the proposed QP-based path smoothing approach, we compare it with an advanced sparse-banded structure-based path smoothing approach SBA [28]. We comprehensively evaluate path smoothing approaches

TABLE I  
QUANTITATIVE STATISTICS OF PATH PLANNING RESULTS IN THE MAZE

		# of expands	Time (secs)	Graph size	Path cost
Test 1	Lattice	155,715	0.115	161,848	291,590
	Ours	<b>140,909</b>	<b>0.097</b>	<b>144,943</b>	291,590
Test 2	Lattice	167,912	0.122	174,356	324,846
	Ours	<b>146,300</b>	<b>0.103</b>	<b>149,912</b>	324,846
Test 3	Lattice	202,680	0.151	210,043	383,376
	Ours	<b>169,949</b>	<b>0.121</b>	<b>173,716</b>	383,376

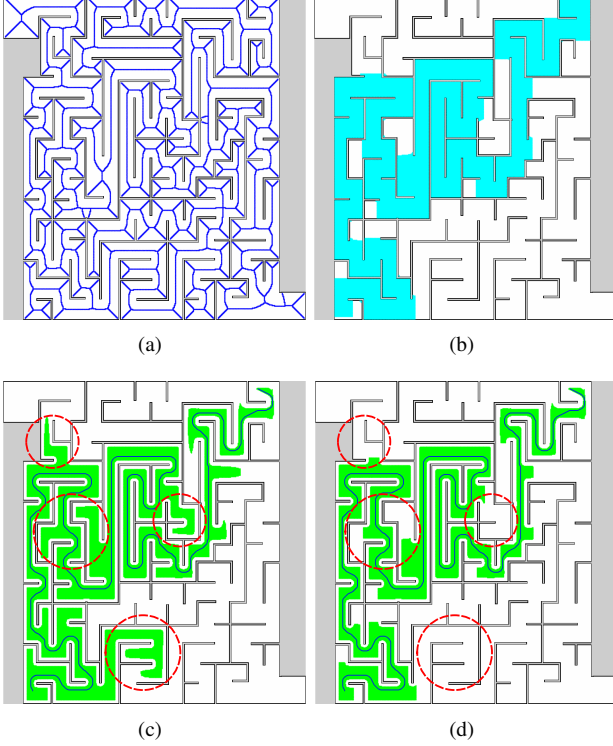


Fig. 6. (a) Grid-based generalized Voronoi diagram. (b) Voronoi corridor. (c) Path planning result of the original state lattice-based path planner. (d) Path planning result of the proposed path planner.

in terms of *travel distance*, *efficiency*, and *smoothness*. In particular, the travel distance  $S$  measures the distance traveled by the robot during the navigation process, the time  $T$  taken by the robot to complete the navigation task is employed to evaluate the motion efficiency, the computational efficiency  $C$  is measured as the time consumption of a single path optimization, and the smoothness is evaluated by the maximum curvature  $K_{\max}$  and mean curvature  $K_{\text{mean}}$ . The curvature is calculated by computing the turning radius of the robot based on the assumption that path vertices are uniformly and densely spread over the path [29]. To satisfy this condition, cubic spline interpolation is utilized to smooth the traveling route of the robot to obtain a continuous curve. Then, we densely sample path vertices on the curve to compute the curvature.

## V. SIMULATIONS

In this section, we verify the applicability of the proposed G<sup>2</sup>VD planner in simulation. The popular Gazebo [37] is

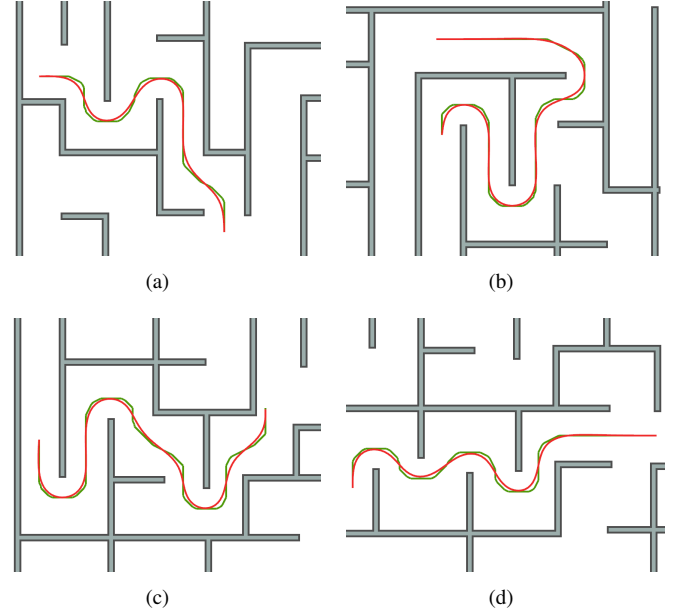


Fig. 7. Searched paths (green) obtained by the proposed path searching approach and corresponding smoothed paths (red) generated by the proposed path smoothing approach in the maze environment.

chosen as the simulator. In this work, we choose the large-scale complex maze<sup>1</sup> scenario designed in [38] for evaluation.

### A. Comparison on Path Searching

As mentioned before, the incrementally updatable GVD construction algorithm described in [31] is employed to generate the grid-based generalized Voronoi diagram of the maze environment, as shown in Fig. 6(a). Furthermore, we randomly select three sets of start and goal configurations in the maze for testing. Both the original state lattice-based path planner and the proposed path planner generate equal quality paths. The quantitative statistics of path searching results in these tests are enumerated in Table I.

The cyan cells in Fig. 6(b) represent the constructed Voronoi corridor in Test 1. Figs. 6(c) and 6(d) show the path planning results of the two path planners in Test 1, respectively, where the green cells denote the visited cells during the searching process. Compared with the original state lattice-based path planner [22], the search space of the proposed path planner is reduced to the Voronoi corridor, thus the search effort spent in those unpromising search areas is significantly saved. As shown in Table I, the number of expanded search states of the proposed path planner decreases by an average of 12.8%, and the computational efficiency is improved by 17.1%. Furthermore, since the search branches for searching in those unpromising search areas are reduced, the number of created nodes in the search graph also decreases. Compared with the original state lattice-based path planner, the graph size of the proposed path planner decreases by an average of 13.9%.

In conclusion, the newly proposed path planner generates equal quality paths with less time and memory consumption than the original state lattice-based path planner.

<sup>1</sup><https://github.com/NKU-MobFly-Robotics/local-planning-benchmark>

TABLE II  
COMPUTATIONAL TIME (IN MILLISECOND) OF PATH SMOOTHING IN THE MAZE

		Mean	Max	Min	Std
Fig. 7(a)	SBA	5.15	6.21	4.99	0.26
	Ours	<b>0.45</b>	<b>0.65</b>	<b>0.42</b>	<b>0.05</b>
Fig. 7(b)	SBA	10.49	12.88	9.77	0.86
	Ours	<b>0.54</b>	<b>0.64</b>	<b>0.37</b>	<b>0.05</b>
Fig. 7(c)	SBA	5.85	7.90	4.55	1.34
	Ours	<b>0.29</b>	<b>0.43</b>	<b>0.27</b>	<b>0.03</b>
Fig. 7(d)	SBA	16.48	17.60	15.72	0.57
	Ours	<b>0.40</b>	<b>0.43</b>	<b>0.39</b>	<b>0.01</b>

TABLE III  
QUANTITATIVE STATISTICS OF LOCAL PLANNING IN THE MAZE

		$S$ (m)	$T$ (s)	$K_{\max}$ ( $m^{-1}$ )	$K_{\text{mean}}$ ( $m^{-1}$ )
Test 1	SBA	41.88	93.85	<b>2.02</b>	0.47
	Ours	<b>40.52</b>	<b>91.44</b>	2.25	<b>0.46</b>
Test 2	SBA	53.45	121.24	2.86	<b>0.58</b>
	Ours	<b>51.47</b>	<b>116.99</b>	<b>2.20</b>	0.59
Test 3	SBA	54.50	123.28	2.13	0.52
	Ours	<b>52.61</b>	<b>119.74</b>	<b>2.08</b>	<b>0.49</b>

### B. Comparison on Path Smoothing

1) *Comparison on Computational Efficiency:* We choose four challenging local scenarios containing continuous S-shaped or U-shaped turns in the maze environment to compare the computational efficiency of path smoothing approaches. For a fair comparison, the proposed path searching approach is employed to generate the reference path for both SBA and the proposed QP-based path smoothing approach. In each scenario, we set the same start and goal configurations and repeat the test 20 times. For testing purposes, we do not limit the length of the initial path for path smoothing, namely, we sample all path points obtained by path searching with an interval of 0.1 m. The searched paths obtained by the proposed path searching approach and the corresponding smoothed paths generated by the proposed QP-based path smoothing approach are shown in green and red in Fig. 7 respectively, and the statistics of the runtime performance are shown in Table II. According to [28], SBA is a soft-constrained path smoothing approach, wherein both the path smoothness and path clearance to obstacles are considered in the optimization formulation. The terms of path clearance to obstacles are non-convex, resulting in the final optimization formulation is also non-convex. While the proposed path smoothing approach formulates the path smoothing problem in the form of convex quadratic programming, and the convexity allows the problem to be solved efficiently. As shown in Table II, the maximum runtime of the proposed path smoothing approach is less than 0.7 ms in all four tests, and the computational efficiency of the proposed approach is 25.3 times faster than that of SBA on average.

2) *Comparison on Motion Efficiency and Motion Smoothness:* To compare the performance of path smoothing ap-

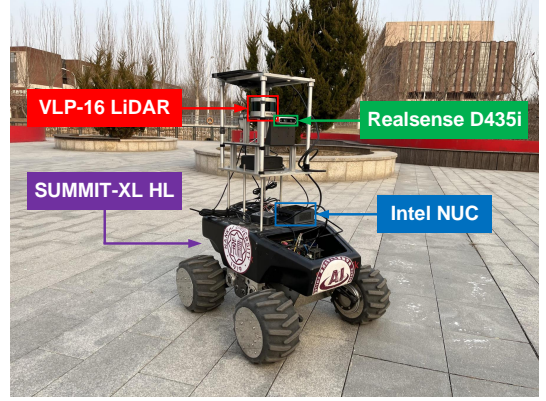


Fig. 8. Our experimental mobile robot SUMMIT-XL HL is equipped with a Velodyne VLP-16 LiDAR, an Intel Realsense D435i depth camera, and an Intel NUC computer. A video showing outdoor navigation on our campus is available at [https://youtu.be/V-S8cS2zv\\_U](https://youtu.be/V-S8cS2zv_U).

proaches in terms of motion efficiency and motion smoothness, the proposed path smoothing approach and SBA are combined with the time-optimal velocity planning algorithm described in [30] to derive a complete local planner, respectively. Furthermore, we randomly select three sets of start and goal configurations in the maze for testing. Table III presents some quantitative statistics of local planning results.

Because the penalty of the deviation from the reference path is considered in the optimization objective of the proposed path smoothing approach, the smoothed path obtained by the proposed approach is close to the path searched by the state lattice-based path planner. And since the path searched by the state lattice-based path planner is optimal in the search space, the path smoothed by the proposed approach is shorter than that of SBA. As shown in Table III, the travel distance of the proposed approach is reduced by an average of 0.96 m, and the motion efficiency is improved by 4.6%. In addition, the smoothness of motion guidance provided by the proposed path smoothing approach is commensurate with that of SBA.

In conclusion, the proposed QP-based path smoothing approach achieves a significant performance improvement in computational efficiency and has a certain improvement in motion efficiency.

## VI. EXPERIMENTS

In this section, outdoor experimental results on our campus are presented to validate the effectiveness of  $G^2VD$  planner.

### A. Experimental Setup

As shown in Fig. 8, the mobile robot SUMMIT-XL HL is used as the experimental platform, which is equipped with a Velodyne VLP-16 LiDAR, an Intel Realsense D435i depth camera, and an Intel NUC computer. The footprint of the robot is approximated as a  $0.8\text{ m} \times 0.8\text{ m}$  square, and the maximum linear velocity is 3.0 m/s. Considering the safety of robot navigation, the upper bound of the linear velocity is set to 1.5 m/s in the experiments.

To generate a prior global map for autonomous navigation, we first employ a LiDAR-inertial odometry algorithm



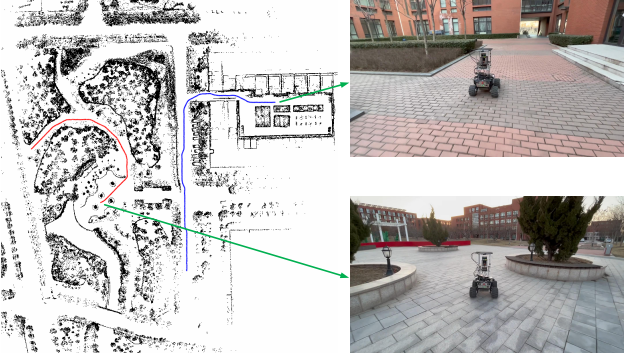


Fig. 9. Occupancy grid map for outdoor navigation. The dimension of the environment is approximately  $210 \text{ m} \times 220 \text{ m}$ . The routes of two sets of robot navigation are colored in red and blue, respectively.

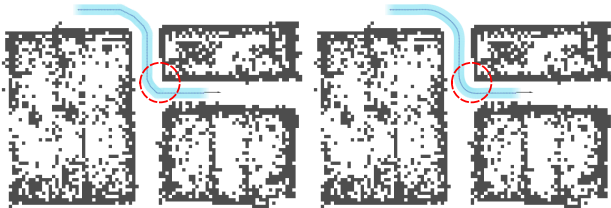


(a)



(b)

(c)



(d)

(e)

Fig. 10. (a) The S-shaped environmental scenario. (b) The path obtained by the original state lattice-based path planner. (c) Smooth path with the path shown in (b) as input. (d) The path obtained by the proposed path planner. (e) Smooth path with the path shown in (d) as input. The light blue strips indicate the footprints of the robot along the path.

described in [39] to build a large-scale 3-D point cloud map. And then, a point clouds segmentation algorithm presented in [40] is used to filter out point clouds that hit the ground and tree canopy. Finally, the filtered point clouds are projected to a 2-D plane to derive traversable regions in the form of the occupancy grid map, as shown in Fig. 9. The dimension of the environment is approximately  $210 \text{ m} \times 220 \text{ m}$ . During robot navigation, the LiDAR-inertial odometry algorithm [39] and the point clouds segmentation algorithm [40] are also utilized to provide state estimation and local traversable regions for the robot, respectively.



Fig. 11. (a) Smooth path without penalizing the deviation from the reference path. (b) Smooth path with penalizing the deviation from the reference path. The light blue strips indicate the footprints of the robot along the path.

TABLE IV  
COMPUTATIONAL TIME (IN MILLISECOND) OF PATH SMOOTHING ON THE CAMPUS

		Mean	Max	Min	Std
Fig. 10	SBA	8.49	10.07	8.09	0.52
	Ours	<b>0.62</b>	<b>0.77</b>	<b>0.56</b>	<b>0.06</b>
Fig. 11	SBA	7.78	9.02	7.23	0.51
	Ours	<b>0.71</b>	<b>0.96</b>	<b>0.65</b>	<b>0.09</b>

### B. Comparison on Path Searching

To validate that the proposed path searching approach can provide sufficient optimization margin for hard-constrained path smoothing approaches, we select an S-shaped scenario shown in Fig. 10(a) to compare path searching approaches. The path shown in Fig. 10(b) is obtained by the original state lattice-based path planner [22]. Since the path clearance is not considered in the original state lattice-based path planner, the searched path is close to the corner of the S-shaped turn, and the corresponding path vertices are fixed in the path smoothing process. As a result, the smoothed path is intuitively rough, as shown in Fig. 10(c). On the contrary, the path clearance is explicitly considered in the proposed path searching approach, thus the searched path shown in Fig. 10(d) has a certain distance from obstacles and provides sufficient optimization margin for the path vertices near the corner. The final smoothed path shown in Fig. 10(e) is much smoother than the path shown in Fig. 10(c), which demonstrates the proposed path searching approach can provide sufficient optimization margin for hard-constrained path smoothing approaches.

### C. Comparison on Path Smoothing

1) *Comparison on Safety*: We select the start and goal configurations shown in Fig. 11 to validate the performance improvement of the proposed path smoothing approach in terms of safety. For a fair comparison, the proposed path searching approach is used to generate the reference path for path smoothing. For testing purposes, we also do not limit the length of the initial path for path smoothing. Generally, hard-constrained path smoothing approaches treat all free space equally, namely, distance from feasible paths to obstacles is ignored. As a result, the optimized path is close to obstacles, as shown in Fig. 11(a). And the penalty of the deviation from the reference path is introduced in the proposed path smoothing

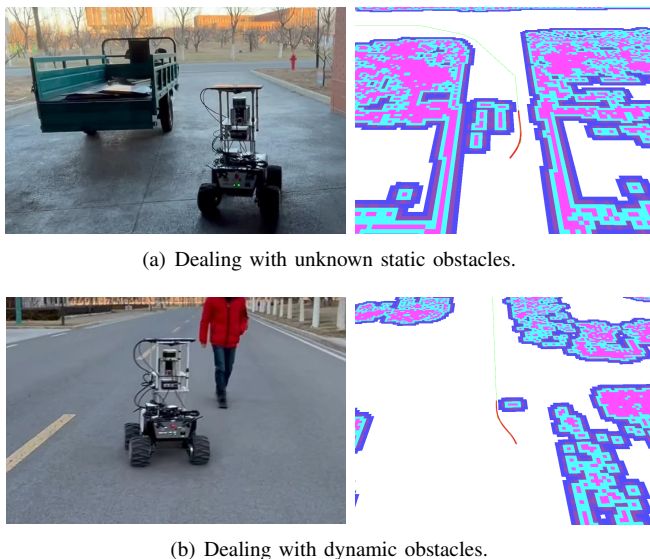


Fig. 12. Screenshots of outdoor navigation results. The green curve denotes the path generated by the proposed path searching approach, and the red curve represents the path smoothed by the proposed path smoothing approach. The pink cells denote obstacles, and the blue cells represent the inflation cells of obstacles according to the footprint of the robot.

approach. Because the reference path searched by the proposed path searching approach has a certain distance from obstacles, the safety of the path is implicitly considered during path smoothing, and the path clearance of the final optimized path is improved, as shown in Fig. 11(b). The minimum distance between the path shown in Fig. 11(a) and obstacles is 0.56 m, which is the same as the circumscribed radius of the robot. While the path clearance of the path shown in Fig. 11(b) is 0.75 m, and the path safety is improved by 33.9%.

2) *Comparison on Computational Efficiency*: We select the start and goal configurations shown in Figs. 10 and 11 to further compare the computational efficiency of path smoothing approaches. For a fair comparison, the proposed path searching approach is employed to generate the reference path for both SBA and the proposed path smoothing approach. In each scenario, we also repeat the test 20 times. The statistics of the runtime performance are shown in Table IV. Thanks to the convexity of the proposed path optimization formulation, the computational efficiency of the proposed path smoothing approach is 12.3 times faster than that of SBA on average.

#### D. Autonomous Navigation

Finally, the proposed path searching and path smoothing approaches are integrated into a real-time navigation system as global and local planners respectively to validate the effectiveness and practicability of the proposed  $G^2VD$  planner. Considering the computational efficiency and sensing range, the length of the initial local path is set to 4.0 m. As illustrated in Fig. 9, we select two sets of different start and goal configurations for outdoor navigation. The total travel distances of these two sets of outdoor navigation are approximately 118.3 m and 165.9 m, respectively.

Here we summarize several representative experimental results of outdoor autonomous navigation to demonstrate the

key characteristics of  $G^2VD$  planner. More details are included in the video.

1) *Dealing With Static Obstacles*: Fig. 12(a) illustrates the scenario with unknown static obstacles. The robot avoids a temporarily parked tricycle smoothly, according to the reliable path smoothing results.

2) *Dealing With Dynamic Obstacles*: Fig. 12(b) shows the scenario with dynamic obstacles. The robot implements fast re-planning and avoids an oncoming person successfully, thanks to the efficient path smoothing approach.

## VII. CONCLUSION

In this paper, an efficient motion planning approach called  $G^2VD$  planner is newly proposed for mobile robots. Based on a grid-based GVD, a new state lattice-based path planner is proposed, in which the search space is reduced to a Voronoi corridor to further improve the search efficiency, along with a Voronoi potential constructed to make the searched path keep a certain distance from obstacles to provide sufficient optimization margin for further path smoothing. And an efficient QP-based path smoothing approach is presented, wherein the clearance to obstacles is considered in the form of the penalty of the deviation from the safe reference path to improve the path clearance of hard-constrained path smoothing approaches. The performance of  $G^2VD$  planner is validated in various complex simulation scenarios and outdoor environments. The results show that the computational efficiency is improved by 17.1% in the path searching stage, and path smoothing with the proposed approach is 25.3 times faster than an advanced sparse-banded structure-based path smoothing approach.

In the future, we plan to challenge  $G^2VD$  planner in extreme scenarios such as large-scale and uneven underground environments. Furthermore, we will also extend the proposed motion planning approach with the theory of partially observable Markov decision process to deal with the uncertainty of dynamic obstacles.

## REFERENCES

- [1] J. Wang, W. Chi, C. Li, and M. Q.-H. Meng, "Efficient robot motion planning using bidirectional-unidirectional RRT extend function," *IEEE Transactions on Automation Science and Engineering*, vol. 19, no. 3, pp. 1859–1868, 2022.
- [2] J. Wang, X. Jia, T. Zhang, N. Ma, and M. Q.-H. Meng, "Deep neural network enhanced sampling-based path planning in 3D space," *IEEE Transactions on Automation Science and Engineering*, vol. 19, no. 4, pp. 3434–3443, 2022.
- [3] X. Zhou, X. Yu, Y. Zhang, Y. Luo, and X. Peng, "Trajectory planning and tracking strategy applied to an unmanned ground vehicle in the presence of obstacles," *IEEE Transactions on Automation Science and Engineering*, vol. 18, no. 4, pp. 1575–1589, 2021.
- [4] Q. Bi, X. Zhang, J. Wen, Z. Pan, S. Zhang, R. Wang, and J. Yuan, "CURE: A hierarchical framework for multi-robot autonomous exploration inspired by centroids of unknown regions," *IEEE Transactions on Automation Science and Engineering*, 2023, doi: 10.1109/TASE.2023.3285300.
- [5] W. Chi, C. Wang, J. Wang, and M. Q.-H. Meng, "Risk-DTRRT-based optimal motion planning algorithm for mobile robots," *IEEE Transactions on Automation Science and Engineering*, vol. 16, no. 3, pp. 1271–1288, 2019.
- [6] J. Wang, W. Chi, C. Li, C. Wang, and M. Q.-H. Meng, "Neural RRT\*: Learning-based optimal path planning," *IEEE Transactions on Automation Science and Engineering*, vol. 17, no. 4, pp. 1748–1758, 2020.

- [7] J. Wang, M. Q.-H. Meng, and O. Khatib, "EB-RRT: Optimal motion planning for mobile robots," *IEEE Transactions on Automation Science and Engineering*, vol. 17, no. 4, pp. 2063–2073, 2020.
- [8] S. M. LaValle, *Planning Algorithms*. Cambridge University Press, 2006.
- [9] L. E. Kavraki, P. Svestka, J.-C. Latombe, and M. H. Overmars, "Probabilistic roadmaps for path planning in high-dimensional configuration spaces," *IEEE Transactions on Robotics and Automation*, vol. 12, no. 4, pp. 566–580, 1996.
- [10] S. M. LaValle and J. J. Kuffner, "Randomized kinodynamic planning," *The International Journal of Robotics Research*, vol. 20, no. 5, pp. 378–400, 2001.
- [11] S. Karaman and E. Frazzoli, "Sampling-based algorithms for optimal motion planning," *The International Journal of Robotics Research*, vol. 30, no. 7, pp. 846–894, 2011.
- [12] O. Khatib, "Real-time obstacle avoidance for manipulators and mobile robots," *The International Journal of Robotics Research*, vol. 5, no. 1, pp. 90–98, 1986.
- [13] A. Ravankar, A. A. Ravankar, Y. Kobayashi, Y. Hoshino, and C.-C. Peng, "Path smoothing techniques in robot navigation: State-of-the-art, current and future challenges," *Sensors*, vol. 18, no. 9, pp. 1–30, 2018.
- [14] C. Rösmann, F. Hoffmann, and T. Bertram, "Kinodynamic trajectory optimization and control for car-like robots," in *Proceedings of the 2017 IEEE/RSJ International Conference on Intelligent Robots and Systems*, 2017, pp. 5681–5686.
- [15] J. Deray, B. Magyar, J. Solà, and J. Andrade-Cetto, "Timed-elastic smooth curve optimization for mobile-base motion planning," in *Proceedings of the 2019 IEEE/RSJ International Conference on Intelligent Robots and Systems*, 2019, pp. 3143–3149.
- [16] J. S. Smith, R. Xu, and P. Vela, "egoTEB: Egocentric, perception space navigation using timed-elastic-bands," in *Proceedings of the 2020 IEEE International Conference on Robotics and Automation*, 2020, pp. 2703–2709.
- [17] C. Rösmann, F. Hoffmann, and T. Bertram, "Integrated online trajectory planning and optimization in distinctive topologies," *Robotics and Autonomous Systems*, vol. 88, pp. 142–153, 2017.
- [18] X. Zhang, A. Liniger, A. Sakai, and F. Borrelli, "Autonomous parking using optimization-based collision avoidance," in *Proceedings of the 2018 IEEE Conference on Decision and Control*, 2018, pp. 4327–4332.
- [19] X. Zhang, A. Liniger, and F. Borrelli, "Optimization-based collision avoidance," *IEEE Transactions on Control Systems Technology*, vol. 29, no. 3, pp. 972–983, 2021.
- [20] Z. Zhu, E. Schmerling, and M. Pavone, "A convex optimization approach to smooth trajectories for motion planning with car-like robots," in *Proceedings of the 2015 IEEE Conference on Decision and Control*, 2015, pp. 835–842.
- [21] C. Liu, C.-Y. Lin, Y. Wang, and M. Tomizuka, "Convex feasible set algorithm for constrained trajectory smoothing," in *Proceedings of the 2017 American Control Conference*, 2017, pp. 4177–4182.
- [22] M. Likhachev and D. Ferguson, "Planning long dynamically feasible maneuvers for autonomous vehicles," *The International Journal of Robotics Research*, vol. 28, no. 8, pp. 933–945, 2009.
- [23] M. Pivtoraiko, R. A. Knepper, and A. Kelly, "Differentially constrained mobile robot motion planning in state lattices," *Journal of Field Robotics*, vol. 26, no. 3, pp. 308–333, 2009.
- [24] D. Ferguson, T. M. Howard, and M. Likhachev, "Motion planning in urban environments," *Journal of Field Robotics*, vol. 25, no. 11–12, pp. 939–960, 2008.
- [25] H. Choset and J. Burdick, "Sensor-based exploration: The hierarchical generalized Voronoi graph," *The International Journal of Robotics Research*, vol. 19, no. 2, pp. 96–125, 2000.
- [26] J. Ziegler, M. Werling, and J. Schroder, "Navigating car-like robots in unstructured environments using an obstacle sensitive cost function," in *Proceedings of the 2008 IEEE Intelligent Vehicles Symposium*, 2008, pp. 787–791.
- [27] D. Dolgov, S. Thrun, M. Montemerlo, and J. Diebel, "Path planning for autonomous vehicles in unknown semi-structured environments," *The International Journal of Robotics Research*, vol. 29, no. 5, pp. 485–501, 2010.
- [28] J. Wen, X. Zhang, H. Gao, J. Yuan, and Y. Fang, "E<sup>3</sup>MoP: Efficient motion planning based on heuristic-guided motion primitives pruning and path optimization with sparse-banded structure," *IEEE Transactions on Automation Science and Engineering*, vol. 19, no. 4, pp. 2762–2775, 2022.
- [29] J. Zhou, R. He, Y. Wang, S. Jiang, Z. Zhu, J. Hu, J. Miao, and Q. Luo, "Autonomous driving trajectory optimization with dual-loop iterative anchoring path smoothing and piecewise-jerk speed optimization," *IEEE Robotics and Automation Letters*, vol. 6, no. 2, pp. 439–446, 2021.
- [30] X. Zhang, J. Wang, Y. Fang, and J. Yuan, "Multilevel humanlike motion planning for mobile robots in complex indoor environments," *IEEE Transactions on Automation Science and Engineering*, vol. 16, no. 3, pp. 1244–1258, 2019.
- [31] B. Lau, C. Sprunk, and W. Burgard, "Efficient grid-based spatial representations for robot navigation in dynamic environments," *Robotics and Autonomous Systems*, vol. 61, no. 10, pp. 1116–1130, 2013.
- [32] P. F. Felzenszwalb and D. P. Huttenlocher, "Distance transforms of sampled functions," *Theory of Computing*, vol. 8, no. 1, pp. 415–428, 2012.
- [33] P. Shen, X. Zhang, and Y. Fang, "Essential properties of numerical integration for time-optimal path-constrained trajectory planning," *IEEE Robotics and Automation Letters*, vol. 2, no. 2, pp. 888–895, 2017.
- [34] P. Shen, X. Zhang, and Y. Fang, "Complete and time-optimal path-constrained trajectory planning with torque and velocity constraints: Theory and applications," *IEEE/ASME Transactions on Mechatronics*, vol. 23, no. 2, pp. 735–746, 2018.
- [35] P. Shen, X. Zhang, Y. Fang, and M. Yuan, "Real-time acceleration-continuous path-constrained trajectory planning with built-in tradeoff between cruise and time-optimal motions," *IEEE Transactions on Automation Science and Engineering*, vol. 17, no. 4, pp. 1911–1924, 2020.
- [36] B. Stellato, G. Banjac, P. Goulart, A. Bemporad, and S. Boyd, "OSQP: An operator splitting solver for quadratic programs," *Mathematical Programming Computation*, vol. 12, no. 4, pp. 637–672, 2020.
- [37] N. Koenig and A. Howard, "Design and use paradigms for Gazebo, an open-source multi-robot simulator," in *Proceedings of the 2004 IEEE/RSJ International Conference on Intelligent Robots and Systems*, 2004, pp. 2149–2154.
- [38] J. Wen, X. Zhang, Q. Bi, Z. Pan, Y. Feng, J. Yuan, and Y. Fang, "MRPB 1.0: A unified benchmark for the evaluation of mobile robot local planning approaches," in *Proceedings of the 2021 IEEE International Conference on Robotics and Automation*, 2021, pp. 8238–8244.
- [39] T. Shan, B. Englot, D. Meyers, W. Wang, C. Ratti, and R. Daniella, "LIO-SAM: Tightly-coupled lidar inertial odometry via smoothing and mapping," in *Proceedings of the 2020 IEEE/RSJ International Conference on Intelligent Robots and Systems*, 2020, pp. 5135–5142.
- [40] H. Liu, R. Song, X. Zhang, and H. Liu, "Point clouds segmentation based on Euclidean clustering and multi-plane extraction in rugged field," *Measurement Science and Technology*, vol. 32, no. 9, pp. 1–14, 2021.



**Jian Wen** received the B.S. degree in automation from Nankai University, Tianjin, China, in 2017, and the Ph.D. degree in control science and engineering from Nankai University, Tianjin, China, in 2022. He is currently working as a Senior Algorithm Engineer at the Group of Autonomous Driving, Xiaomi EV Company Limited.

His research interests include behavioral reasoning, decision making, and motion planning for autonomous passenger vehicles.





**Xuebo Zhang** (M'12–SM'17) received the B.Eng. degree in automation from Tianjin University, Tianjin, China, in 2006, and the Ph.D. degree in control theory and control engineering from Nankai University, Tianjin, China, in 2011.

From 2014 to 2015, he was a Visiting Scholar with the Department of Electrical and Computer Engineering, University of Windsor, Windsor, ON, Canada. He was a Visiting Scholar with the Department of Mechanical and Biomedical Engineering, City University of Hong Kong, Hong Kong, in 2017.

He is currently a Professor with the Institute of Robotics and Automatic Information System, Nankai University, and Tianjin Key Laboratory of Intelligent Robotics, Nankai University. His research interests include planning and control of autonomous robotics and mechatronic system with focus on time-optimal planning and visual servo control; intelligent perception including robot vision, visual sensor networks, SLAM; reinforcement learning and game theory.

Dr. Zhang is a Technical Editor of *IEEE/ASME Transactions on Mechatronics* and an Associate Editor of *ASME Journal of Dynamic Systems, Measurement, and Control*.



**Yongchun Fang** (S'00–M'02–SM'08) received the B.S. degree in electrical engineering and the M.S. degree in control theory and applications from Zhejiang University, Hangzhou, China, in 1996 and 1999, respectively, and the Ph.D. degree in electrical engineering from Clemson University, Clemson, SC, in 2002.

From 2002 to 2003, he was a Post-Doctoral Fellow with the Sibley School of Mechanical and Aerospace Engineering, Cornell University, Ithaca, NY, USA. He is currently a Professor with the

Institute of Robotics and Automatic Information System, Nankai University, Tianjin, China. His research interests include visual servoing, AFM-based nano-systems, and control of underactuated systems including overhead cranes.



**Qingchen Bi** received the B.S. degree in detection guidance and control technology from Northwestern Polytechnical University, Xi'an, China, in 2021, where he is currently pursuing the M.S. degree in control science and engineering with the Institute of Robotics and Automatic Information System, Nankai University, Tianjin, China.

His research interests include mobile robot motion planning, autonomous exploration.



**Hui Liu** received the B.S. degree in intelligence science and technology from Hebei University of Technology, Tianjin, China, in 2019, and the M.S. degree in control science and engineering with the Institute of Robotics and Automatic Information System, Nankai University, Tianjin, China, in 2022.

His research interests include simultaneous localization and mapping (SLAM), calibration.



**Jing Yuan** (M'12) received the B.S. degree in automatic control, and the Ph.D. degree in control theory and control engineering from Nankai University, Tianjin, China, in 2002 and 2007, respectively.

Since 2007, he has been with the College of Computer and Control Engineering, Nankai University, where he is currently a Professor. His current research interests include robotic control, motion planning, and SLAM.